AIAA JOURNAL
Vol. 38, No. 11, November 2000

Mean Flowfield Scaling of Supersonic Shock-Free Three-Dimensional Turbulent Boundary Layer

W. Konrad* and A. J. Smits†
Princeton University, Princeton, New Jersey 08540
and
D. Knight‡
Rutgers University, Piscataway, New Jersey 08854

The mean flowfield of a three-dimensional supersonic turbulent boundary layer, generated by a 20-deg isentropic compression, was studied experimentally and numerically. Experimental data include surface flow visualization, wall static pressures, surface skin friction, and surveys of pitot pressures, yaw angles, and static pressures. Earlier published comparisons with data computed from the three-dimensional Reynolds-averaged compressible Navier–Stokes equations with an algebraic turbulence eddy viscosity closure show good agreement within experimental and computational uncertainties. Focus of the current work is the presentation of different scalings of the experimental data and the proposal of a new model for the mean flowfield scaling. Comparison to a subsonic three-dimensional boundary layer is made for this new scaling law.

Nomenclature

A, e	=	constants in Johnston triangular model
C_f	=	skin-friction coefficient
Q^{++}	=	van Driest-transformed resultant velocity
Re_θ	=	Reynolds number based on momentum thickness
$T_w / T_{0\infty}$	=	total temperature ratio across the boundary layer
U	=	mean velocity in the direction of the local freestream
U_e	=	mean edge velocity in the direction of the local freestream
U_∞	=	incoming freestream mean velocity
u_τ	=	friction velocity
W	=	mean velocity parallel to the wall and perpendicular to U
X, Y, Z	=	Cartesian tunnel coordinates as indicated in Fig. 1
Y^{++}	=	van Driest-transformed inner coordinate
γ	=	local flow angle
γ_e	=	flow angle in the freestream
γ_w	=	flow angle at the wall
$\Delta X, \Delta Y, \Delta Z$	=	computational grid spacing
ΔY^+	=	distance from the wall in wall units
δ_{99}	=	local boundary-layer thickness
δ_∞	=	incoming boundary-layer thickness
δ^*	=	displacement thickness
θ	=	momentum thickness
ν_w	=	kinematic viscosity evaluated at the wall

Introduction

WE present the results of a combined experimental and computational study of a pressure-driven, three-dimensional supersonic turbulent boundary layer generated by a curved fin placed normal to the wall where the incoming two-dimensional boundary layer developed (Fig. 1). We are primarily concerned with the scaling of the mean velocity profiles. The curvature of the fin was chosen so that the compression waves focused to a point well away from the surface of the fin, and consequently, the flow is shock free. The strength of the spanwise and streamwise gradients increased progressively through the interaction, so that the degree of three dimensionality, that is, the level of yaw, increased in the same way. The freestream incoming Mach number is 2.87, and the final turning angle is 20 deg, similar to previous studies of the three-dimensional boundary layer generated by sharp, plane fins. The near flowfield of the curved fin is such that static pressures, static pressure gradients, and streamline curvatures all increase continuously and gradually throughout the entire flowfield, in the streamwise and spanwise directions. This is in contrast to the more commonly studied shock-wave/boundary-layer interactions of comparable ultimate pressure rise.

The experimental and numerical research programs were conducted in parallel. First, the conditions of the incoming wind tunnel floor boundary layer were established experimentally. With these survey data, computations were performed using a Reynolds-averaged Navier–Stokes code and mean flowfield data were measured, that is, surface flow visualization, wall static pressures, Preston tube data, yaw angles, and pitot and static pressure surveys. Then, the experimental data were compared with the computations, and after establishing confidence in the numerical results, the mean flowfield structure was analyzed in detail using both the experimental and numerical data.

The results were reported by Konrad et al.,[1] who found that a line of convergence appeared in the surface flow visualization that conveniently divided the flowfield into two regions. The upstream region could be further subdivided into a small crossflow region and an upstream convergence region. The small crossflow region is characterized by small yaw angles (less than 10 deg). In the upstream convergence region, the crossflow angles increased to about 20 deg, and the flow near the wall experienced near-wall retardation similar to that seen in other adverse pressure gradient flows. Pitch angles were very small everywhere, and the local boundary layer thickness remained almost constant throughout the interaction, so that the streamline curvature was virtually confined to horizontal planes (called in-plane curvature).

The strongest effects of three dimensionality were seen in the downstream convergence region. The velocity in the outer part of the layer decreases due to the pressure gradients along the mean streamline, while the near-wall velocity profile is much fuller because high-momentum fluid from the upstream boundary layer is drawn closer to the wall as the low-momentum fluid originally near the wall is removed by the action of the spanwise pressure gradients. We discuss the scaling of the mean velocity profiles in detail. In particular,

Received 15 July 1997; revision received 6 March 2000; accepted for publication 29 April 2000.

*Graduate Research Assistant, Mechanical and Aerospace Engineering Department; currently Manager Experimental Vehicles, BMW AG, TI-30, 80788 Munich, Germany.

†Professor and Chairman, Department of Mechanical and Aerospace Engineering. Associate Fellow AIAA.

‡Professor, Department of Mechanical and Aerospace Engineering. Associate Fellow AIAA.

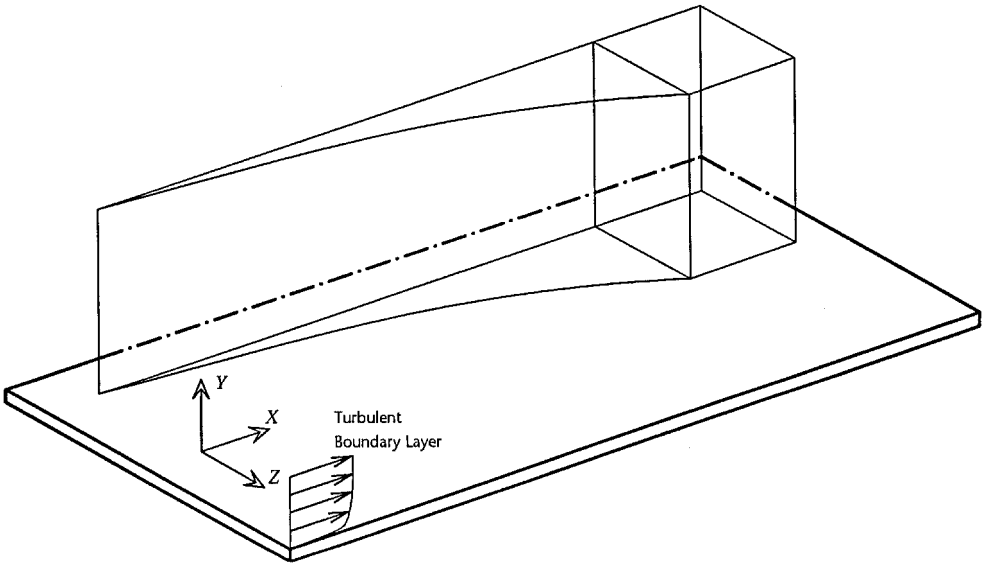

Fig. 1 Experimental setup.

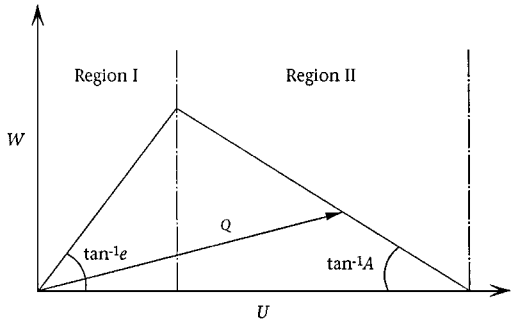

Fig. 2 Johnston[2] triangular model 1.8.

we are concerned with applicability of the Johnston[2] triangular model, as understood from the experimental and computational results. Johnston suggested that the velocities in a three-dimensional boundary layer in incompressible flow are independent of the wall distance and scale according to

$$W/U_e = e(U/U_e), \qquad W/U_e = A[1-(U/U_e)]$$

in regions I and II, respectively, of the polar representation of the velocity profile shown in Fig. 2. Regions I and II are defined by the vertices of the triangle and the slopes, which depend on the parameters A and e, which are constants for a given location. In region I, the velocities are collateral, that is, the yaw angles are constant. The parameter e is found by plotting the velocity profiles. An observer moving with the freestream velocity would see the velocity vectors in the outer part of the boundary layer point at a plane that moves laterally and rotates with respect to the wall.

Perry and Joubert[3] used a first-approximation analysis to show that Johnston's[2] triangular plot is mainly a consequence of the geometry of the apparatus. For the velocity profile to follow a triangular distribution, then 1) the magnitude of the velocity gradient in the outer region of the boundary layer should be of order U_e/L (L being a typical streamwise length scale), rather than U_e/δ, and 2) the velocity defects in the spanwise and streamwise directions need to be small, of order $U_e\delta/L$. It can be expected, therefore, that triangular scaling will hold only in regions of small crossflow.

Several attempts have been made to derive a law of the wall for three-dimensional boundary layers. Pierce and McAllister,[4] in an extensive review of the literature, concluded that all current models for subsonic flow are restricted to small crossflow. The primary difficulties in extending this work to higher crossflow angles appear to be the departures from an isotropic eddy viscosity and the identification of an appropriate velocity scale. For example, when the crossflow angles are small, there is little distinction between the friction velocity based on the component of velocity in the freestream direction or on the velocity magnitude itself. As the crossflow increases, the discrepancy will obviously grow.

In the supersonic regime, our understanding of three-dimensional boundary layers is even more rudimentary. Past research has focused on shock-generated interactions,[5,6] and few studies of shock-free three-dimensional boundary layers have been carried out. The most interesting work was done by Hall[7] and Demetriades and McCullough.[8] Hall[7] reported extensive mean measurements in a Mach 1.6–2.0 wavy passage flow, where there was a reversal of direction of the crossflow, and found that the Johnston[2] triangular plot did not fit the data. Demetriades and McCullough[8] generated a shock-free three-dimensional boundary layer using a curve twisted-edge model in a Mach 3 flow. The model was designed to achieve zero streamwise pressure gradient while keeping the transverse pressure gradient constant. Again, Johnston's[2] triangular plot did not fit the data, but the data followed van den Berg's[9] extended law of the wall in the near-wall region. All other experiments reported in the literature on supersonic three-dimensional boundary layers studied flows where the three dimensionality was induced by a shock or a shock-wave/boundary-layer interaction, and therefore the present study was undertaken to help improve our basic understanding of shock-free three-dimensional boundary layers.

Experiment

All experiments on the three-dimensional curved fin flow were performed in the high Reynolds number supersonic blowdown wind tunnel at the Princeton Gas Dynamics Laboratory. The freestream had a Mach number of 2.87 (±1%), a total pressure of 6.89×10^5 N/m^2 (±1%) (100 psi), and a nominal total temperature of approximately 265 K (±2%). Wall conditions were nearly adiabatic ($T_w/T_{0_\infty} \approx 1.04$).

To determine the incoming boundary-layer conditions, five surveys were taken at different spanwise locations using a high-resolution pitot probe with a flattened tip height of only 0.635 mm (0.025 in.). The boundary-layer parameters on the centerline are listed in Table 1. Some spanwise nonuniformity was found, and it was probably due to the inlet to the tunnel nozzle and the growth of the sidewall boundary layers. The divergence from two dimensionality is relatively small (less than ±5% in C_f over $5\delta_\infty$) and, thus, was not expected to influence the results of the current investigation significantly. At all survey stations, the boundary layer was typical of a high Reynolds number, supersonic, self-preserving flow.

The experimental setup is shown in Fig. 1. A Cartesian coordinate system was used, so that the origin was located at the leading edge of the fin, on the centerline of the test section [76.2 mm (3 in.) from the fin leading edge], with X as the streamwise direction and Y as the wall-normal direction. The fin was designed to have the inviscid

focal point of the compression wave system at 0.229 m (9 in.) spanwise from the leading edge so that no shock waves would be generated in the 0.203 × 0.203 m (8 × 8 in.) tunnel test section. The computed streamwise location of the focal point was 0.615 m (24.2 in.), and the streamwise length of the fin was 0.476 m (18.7 in.). The asymptotic fin angle was 20 deg, and the line of convergence in the surface flow visualization was located at $X = 0.36$ m (14.2 in.) on the centerline. The work of Konrad[10] contains all input data necessary for computations.

Figure 3 shows a top view of the complete test section as it was used for all experiments. A sidewall control plate was installed to minimize sidewall boundary-layer separation. Eight different survey plug positions were used for flowfield measurements, evenly spaced at 63.5 mm (2.5 in.) along the centerline of the tunnel. The plug diameter was 50.8 mm (2 in.). To be able to access a larger number of stations, the model could be mounted in several streamwise positions. At the length Reynolds number used in the experiment, the boundary-layer development was very slow, and moving the model was judged to be acceptable. The plug was designed to accommodate all of the different survey instruments (Preston, three-hole pitot, static probes), and it could be rotated during a survey so that the probes could be aligned with the local flow direction. In addition, the plug housed a wall static pressure tap that was particularly useful when aligning probes.

For all boundary-layer surveys, a three-hole pitot (Cobra) probe determined yaw angles and pitot pressures at each location by nulling the pressure differential of the outer tubes. The pitot pressure uncertainties are expected to be within 2%, and small misalignments of the probe did not affect the reading of the pitot pressure. Pitch angles were assumed to be small and, therefore, were not measured. The highest pitch angle anywhere in the flowfield found from the computed results was 5 deg, but no pitch angle greater than 1 deg was found at the centerline survey locations. The uncertainties in initial alignment were estimated to be less than 1 deg so that subsequent adjustments of the data were not necessary.

Table 1 Boundary-layer characteristics

Parameter	Value
δ_∞	25 mm ±5%
δ^*	6.1 mm ±2%
θ	1.1 mm ±3%
Re_θ	84,000 ±5%
C_f	0.00104 ±5%

The static surveys were made after the yaw angles were established, and the static probe was simply yawed to the predetermined flow direction at a given height. The static probe was relatively insensitive to misalignment; Liepmann and Roshko[11] indicate a range of ±5 deg from the local flow direction in which the static pressure is read with errors of less than 1%. Further details are given by Konrad.[10]

Computations

The three-dimensional Reynolds-averaged compressible Navier–Stokes equations were employed with turbulence modeled with the algebraic turbulent eddy viscosity model of Baldwin and Lomax.[12] Previous computations[13] of the three-dimensional sharp fin at comparable conditions have demonstrated that the mean flowfield structure is principally rotational and inviscid (and hence insensitive to the turbulence model employed) except in a very narrow region near the surface.

The vectorized hybrid explicit–implicit numerical algorithm of Knight[14] was utilized to integrate the governing equations in time from an assumed initial condition until steady state was achieved. The condition for convergence was an average relative change in the flowfield variables of less than 1% over one characteristic time t_c (the physical time required for the flow to traverse the computational domain in the general streamwise direction).

A total of 107,325 grid points were employed. The streamwise grid spacing was $\Delta X = 0.5\delta_\infty$, one-half of the value employed in previous computations of the three-dimensional sharp fin under similar flow conditions.[15,16] The computed results for the three-dimensional sharp fin were found in good agreement with experiment. The grid points in the Y–Z planes were stretched geometrically with sufficient resolution near the surfaces to resolve the boundary layers on the flat plate and fin. The maximum value was $\Delta Y^+ = \Delta Y u_\tau / \nu_w = 0.89$, which is sufficient for accurate resolution of the viscous sublayer for an algebraic turbulence model. The number of grid points in the Y direction within the upstream boundary layer was 32, more than typically used for previous three-dimensional single fin computations. Outside the region of three-dimensional flow, the maximum value was $\Delta Y = \Delta X = 0.5\delta_\infty$. This is comparable to the value employed for the three-dimensional sharp

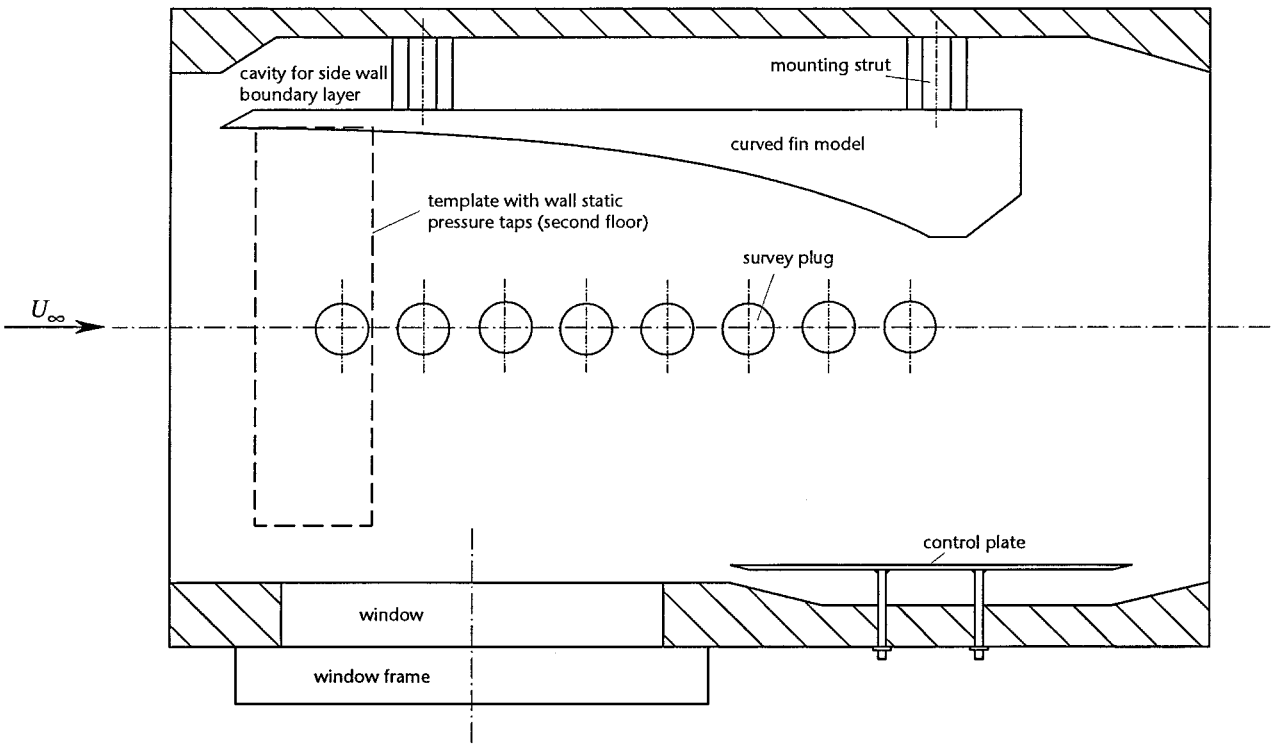

Fig. 3 Top view of experimental test section.

fin. The boundary layer on the curved fin was transitional in the experiment but modeled as fully turbulent from the leading edge in the computations. Although the fin boundary layer has negligible influence on the interaction (except in the immediate vicinity of the corner formed by the fin and the flat plate), a reasonably accurate grid was employed with minimum spacing. The maximum value ΔZ was $0.49\delta_\infty$, which is comparable to the maximum value of ΔX and ΔY and the value employed for the three-dimensional sharp fin.

The freestream conditions and the total temperature boundary-layer profile were taken from the experiment. The upstream boundary-layer profile for the computations was obtained from a boundary-layercode (using the same turbulence model) by matching the experimental displacement thickness δ^*. The upstream profile was obtained from the boundary-layercalcultion taking into consideration the distance from the measurement location ($X = 96.5$ mm) (3.8 in.) to the location of the upstream boundary of the computations. At the location of the measurement of δ^*, the computed momentum thickness θ was 1.28 mm (0.05 in.) (9.6% above the average experimental value), and the computed skin-friction coefficient was $C_f = 0.00097$ (13.4% below the average experimental value). This agreement is typical of previous comparisons with experiment. (Further details are given by Konrad et al.[1])

Results

The van Driest[17] transformation was used to map the compressible mean velocity field into the incompressible domain. Note that the transformation was applied to the magnitude of the velocity vector in the local flow direction rather than for the streamwise component alone. The profiles at four different stations are plotted in Fig. 4. The friction velocities used in this representation were found by the Clauser chart method,[18] that is, by fitting the overlap region to the standard logarithmic law using $\kappa = 0.41$ and an additive constant of 5.2. This approach was also taken by Hornung and Joubert[19] in subsonic flow. The wall shear stress was also found using Preston tubes.[20] In three-dimensional supersonic boundary layers with considerable crossflow, it seems possible to use Preston tubes, mainly because the region very close to the wall displays quasi-two-dimensional behavior. In the wall region, due to viscosity and high-turbulence intensity, adjustment to pressure gradients occurs quickly, and the application of the law of the wall is often still a good approximation. For example, Kim et al.[21] found good agreement between the results obtained using Preston tubes and a direct measurement of the shear stress using laser interferometry in a three-dimensional shock-wave/boundary-layer interaction generated by a 10-deg sharp fin at Mach 3.

Although the accuracy of the derived shear stress is in question, the agreement with the Preston tube method was within ±10%, as shown in Fig. 5. A sharp rise in the skin friction is observed at the location corresponding to the location of the line of convergence. The agreement with the computation is also reasonably satisfactory, especially in the downstream convergence region. The largest discrepancies are found in the upstream convergence region, where the computational results fall below the experimental values by as much as 30%.

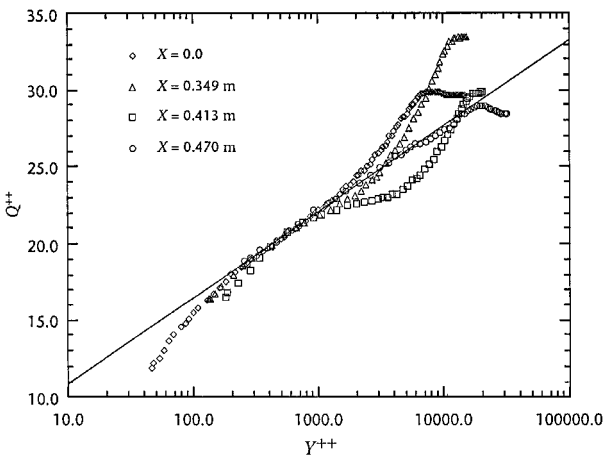

Fig. 4 van Driest[17] transformed velocity profiles in inner coordinates.

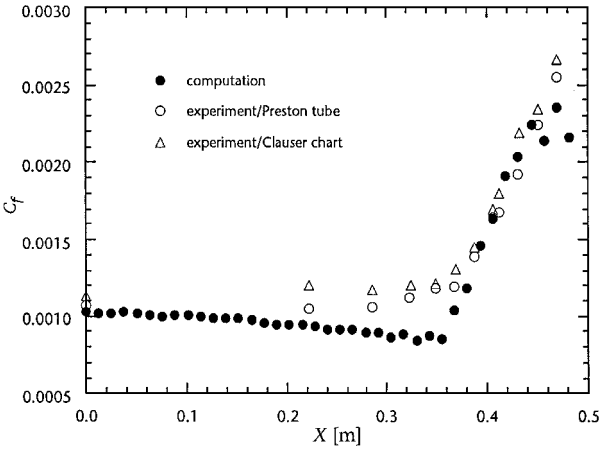

Fig. 5 Skin-friction coefficients along the centerline 3.17.

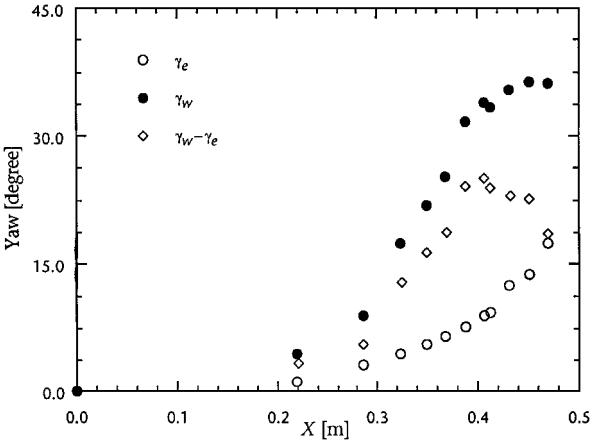

Fig. 6 Experimental yaw angles.

The profiles themselves all show a logarithmic region, even in the highly distorted downstream parts of the flowfield. At $X = 0.349$ m (13.7 in.), a slight dip below the logarithmic law is seen in the velocity profile, whereas at $X = 0.413$ m (16.3 in.) a very large dip has developed. These dips are typically associated with two-dimensional flows with concave streamline curvature. Here, they most likely indicate the different history effects experienced by the inner and outer parts of the boundary layer (see subsequent discussion). Farther downstream, however, the boundary layer starts to recover, and at $X = 0.470$ m (18.5 in.) the dip in the outer part of the boundary layer has practically disappeared.

To demonstrate the increasing three dimensionality in the mean flowfield, Fig. 6 shows the experimental yaw angles along the centerline. Crossflow is defined here as the difference between the wall turning angle γ_w and the freestream turning angle γ_e. The crossflow increases steadily until it reaches a maximum at about $X = 0.413$ m (16.3 in.), where it drops slightly. Note that the small crossflow limit (for example, $\gamma_w - \gamma_e < 10$ deg) is only met by the profile at $X = 0.222$ m (8.7 in.). There are some experimental difficulties in determining accurate yaw angles near the wall, but within the experimental uncertainty, the yaw angles in the near-wall region ($Y^{++} < 1000$) are approximately constant, that is, the flow is nearly collateral. This region also corresponds to the region where the velocity profiles display a logarithmic variation with wall distance.

The experimental streamwise and spanwise velocity components are plotted in Figs. 7 and 8, respectively, as a function of Y. The natural normalizing parameter for Y would be the local boundary-layer thickness, but due to the difficulty in determining the edge state and the absence of simple similarity parameters, we decided to plot Y for all profiles without a normalizing parameter. The velocities are normalized by the local freestream. The line of convergence is at $X = 0.36$ m (14.2 in.) and $Z = 0$.

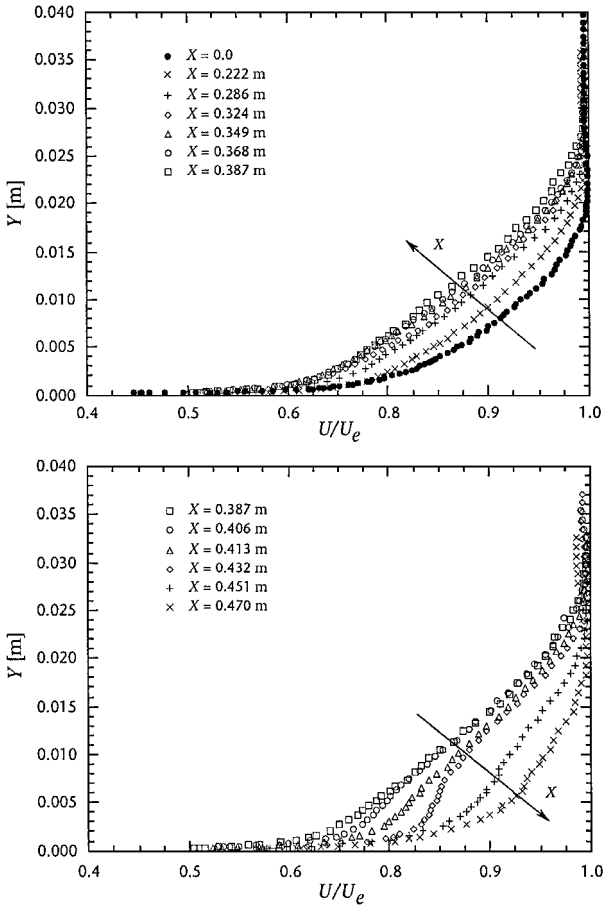

Fig. 7 Streamwise velocity profiles along the centerline.

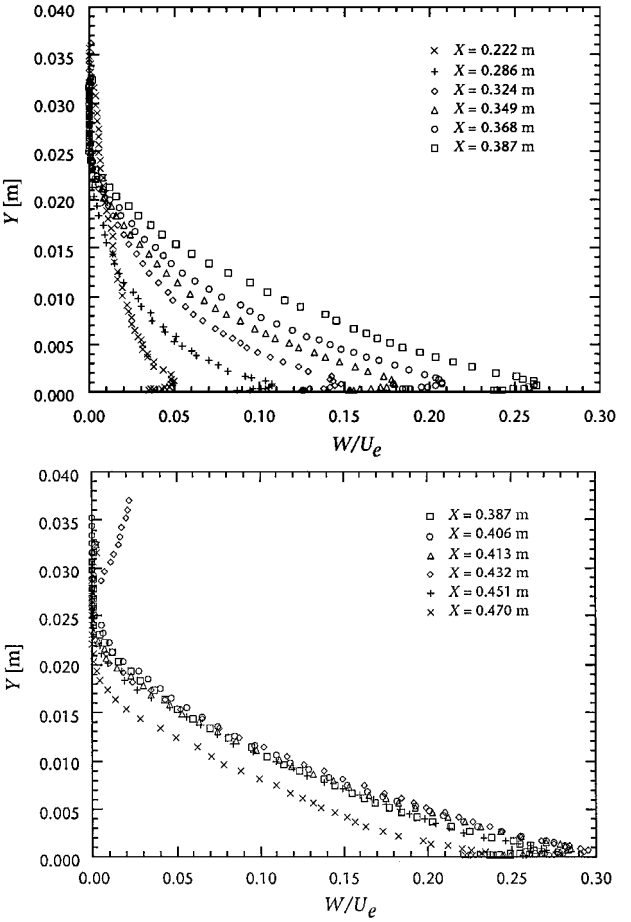

Fig. 8 Spanwise velocity profiles along the centerline.

In Fig. 7, it is seen the streamwise velocities upstream of the convergence line are increasingly retarded as X increases, whereas downstream of the line of convergence the three-dimensional effects dominate and the near-wall streamwise velocities increase as a result of the entrainment of high-momentum fluid. In contrast to two-dimensional adverse pressure gradient flows, the velocity profiles downstream of the line of convergence are accelerated, although the spanwise and streamwise pressure gradients continue to increase monotonically with streamwise distance. Figure 8 shows the spanwise components, and here the maximum velocity is reached at $X = 0.432$ m (17 in.). Farther downstream, the relaxation of the boundary layer leads to a decrease in the spanwise velocity components.

The velocity components are shown in polar plots in Fig. 9. As mentioned earlier, no generally applicable scaling law exists that collapses three-dimensional boundary-layer velocity profiles. Certainly the profiles in the downstream locations do not collapse in this polar representation. Under certain geometrical flow conditions, however, the data in the upstream part of the flowfield can be collapsed. This is possible in the farthest upstream region, where the behavior is close to that of two-dimensional boundary layers. In Fig. 10 the polar plot for $X = 0.222$ m (8.7 in.) is shown, and it follows approximately the Johnston triangular model.[2] The computed velocity profile is more convincing than the experimental one primarily because the experimental surveys in the upstream region fail to resolve small changes in flow direction. That we can expect the Johnston triangular model to hold in the small crossflow region (up to about 10-deg crossflow) can be shown by a small perturbation analysis of the mass-averaged continuity and momentum equations, basically following the incompressible analysis of Perry and Joubert,[3] who found that the Johnston[2] triangle is a consequence of certain flow geometries. It can be assumed that in the outer part of the boundary layer the mass-averaged and Reynolds-averaged analyses do not differ too much because in this region the turbulence Mach numbers are small.

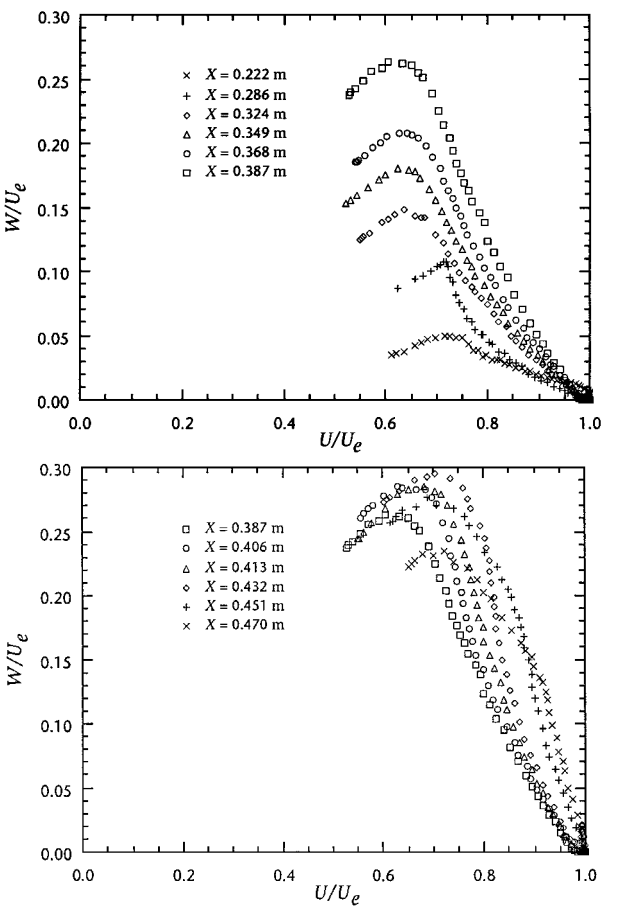

Fig. 9 Polar plot of velocity profiles.

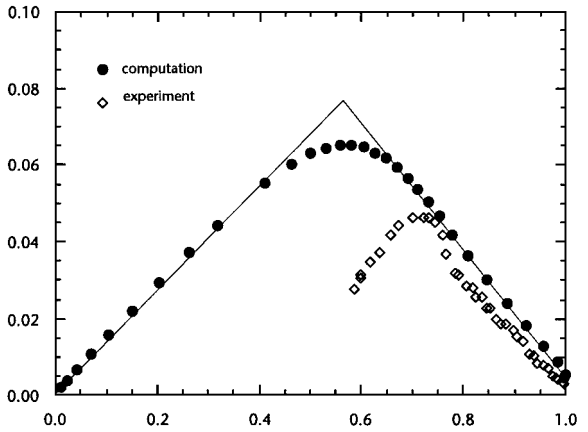

Fig. 10 Johnston[2] triangular model for $X = 0.222$ m.

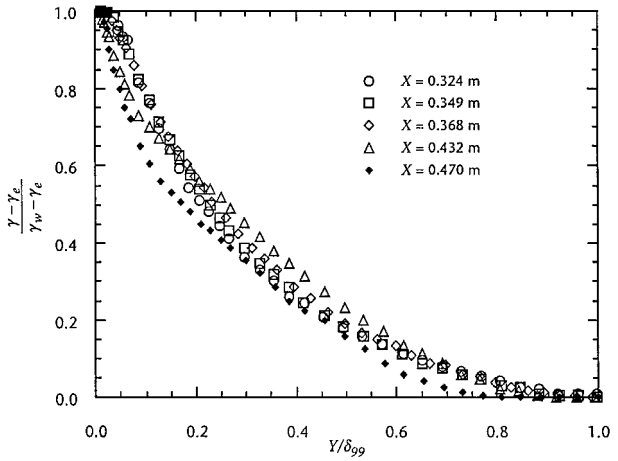

Fig. 11 Crossflow profiles scaled by the maximum crossflow.

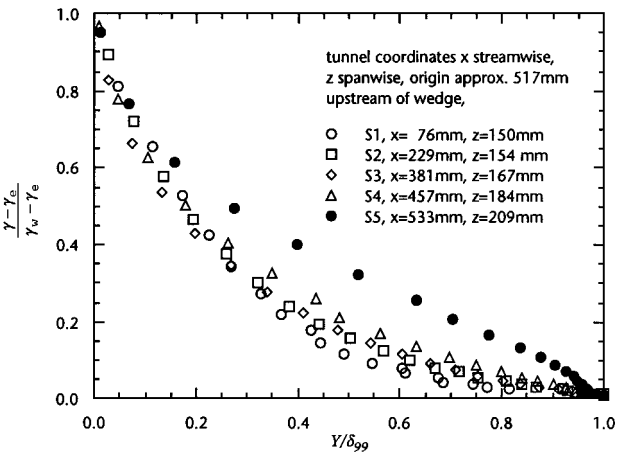

Fig. 12 Crossflow profiles scaled by the maximum crossflow for Anderson and Eaton.[22]

A different scaling can be tried. The shape of the polar plots is generally rather similar, and the peak value simply corresponds to the point of maximum crossflow, that is, $(W/U)_{\max}$. This encourages us to try plotting the yaw profiles as $(\gamma - \gamma_e)/(\gamma_w - \gamma_e)$ vs Y/δ_{99}. The vertical distance from the wall where 99% of the freestream total pressure is reached, δ_{99}, is determined as precisely as possible from the total pressure surveys. The collapse shown in Fig. 11 is very impressive and suggests a universal crossflow distribution for three-dimensional flows. To test the universality of this crossflow distribution, we plotted the data obtained by Anderson and Eaton[22] in a subsonic three-dimensional boundary layer generated by a 90-deg wedge on a flat plate. The cross-flow angles ranged from 3.9 to 46.3 deg, and the results shown in Fig. 12 indicate that the scaling we suggest here works well for this experiment, except for the largest crossflow case. The universal curves in Figs. 11 and 12 also agree reasonably well, and this new scaling appears promising. Further work will need to be done to confirm its general applicability.

Summary

Three distinct flow regimes were identified in the interaction. The velocity profiles continued to display a logarithmic region in all three flow regimes, and it followed the standard logarithmic law, given the uncertainties in finding the wall stress. The logarithmic region corresponded to the region of the velocity profile where the yaw angles were approximately constant, that is, where the flow is collateral. In the outer flow, a dip below the logarithmic region is seen to develop, similar to what is seen in supersonic flows with adverse pressure gradient and concave streamline curvature. The separation of the upstream region in two subdomains (the small crossflow region and the upstream convergence region) is somewhat arbitrary and depends on the definition of small crossflow. Here we took 10 deg as the maximum small crossflow angle, although another criterion could be the applicability of the Johnston triangular model, as we saw. The triangular scaling did not extend downstream of the small crossflow region. A new scaling is proposed for the yaw profiles, where we found similarity of the crossflow profile when it is scaled by the maximum crossflow.

Acknowledgments

The work was sponsored by the Air Force Office of Scientific Research under Grants 89-0033 and 86-0266 monitored by L. Sakell. Supercomputer resources were provided by NASA Ames Research Center. Analysis of the flowfield was performed at the College of Engineering Supercomputer Remote Access Facility sponsored by Rutgers University. Analysis of the flowfield structure was performed at and sponsored by Princeton University.

References

[1] Konrad, W., Smits, A. J., and Knight, D., "A Combined Experimental and Numerical Study of a Three-Dimensional Supersonic Turbulent Boundary Layer," *Experimental Thermal and Fluid Science*, Vol. 9, 1994, pp. 156–164.

[2] Johnston, J. P., "On the Three-Dimensional Turbulent Boundary Layer Generated by Secondary Flow," *Journal of Basic Engineering, Series D*, Vol. 82, 1960, pp. 233–248.

[3] Perry, A. E., and Joubert, P. N., "A Three-Dimensional Turbulent Boundary Layer," *Journal of Fluid Mechanics*, Vol. 22, 1965, pp. 285–304.

[4] Pierce, F. J., and McAllister, J. E., "Near-Wall Similarity in a Shear-Driven Three-Dimensional Turbulent Boundary Layer," *Journal of Fluids Engineering*, Vol. 105, 1983, pp. 263–269.

[5] Settles, G., and Dolling, D., "Swept Shock Wave Boundary-Layer Interactions," *Tactical Missile Aerodynamics*, Vol. 104, 1986, pp. 297–379.

[6] Settles, G., and Dolling, D., "Swept Shock/Boundary-Layer Interactions–Tutorial and Update," AIAA Paper 90-0375, 1990.

[7] Hall, M. G., "Experimental Measurements in a Three-Dimensional Turbulent Boundary Layer in Supersonic Flow," AGARDograph 97, Pt. 2, May 1965, pp. 829–853.

[8] Demetriades, A., and McCullough, G., "Mean-Flow Measurements in a Supersonic Three-Dimensional Turbulent Boundary Layer," *Journal of Fluid Mechanics*, Vol. 156, 1985, pp. 401–418.

[9] van den Berg, B., "A Three-Dimensional Law of the Wall for Turbulent Shear Flows," *Journal of Fluid Mechanics*, Vol. 70, 1975, pp. 149–160.

[10] Konrad, W., "A Three-Dimensional Supersonic Turbulent Boundary Layer Generated by an Isentropic Compression," Ph.D. Dissertation, Dept. of Mechanical and Aerospace Engineering, Princeton Univ., Princeton, NJ, 1993.

[11] Liepmann, H. W., and Roshko, A., *Elements of Gasdynamics*, Wiley, New York, 1957.

[12] Baldwin, B., and Lomax, H., "Thin Layer Approximation and Algebraic Model for Separated Turbulent Flows," AIAA Paper 78-257, 1978.

[13] Knight, D., Horstman, C., Shapey, B., and Bogdonoff, S., "The Flowfield Structure of the 3D Shock Wave Boundary Layer Interaction Generated by a 20 Deg Sharp Fin at Mach 3," AIAA Paper 86-0343, 1986.

[14] Knight, D., "Hybrid Explicit–Implicit Numerical Algorithm for the Three-Dimensional Compressible Navier–Stokes Equations," *AIAA Journal*, Vol. 22, 1984, pp. 1056–1061.

[15] Knight, D., Horstman, C., Shapey, B., and Bogdonoff, S., "Structure of Supersonic Turbulent Flow Past a Sharp Fin," *AIAA Journal*, Vol. 25, 1987, pp. 1331–1337.

[16] Knight, D., Horstman, C., Ruderich, R., Mao, M.-F., and Bogdonoff, S., "Supersonic Turbulent Flow Past a 3D Swept Compression Corner at Mach 3," AIAA Paper 87-0551, 1987.

[17] van Driest, E. R., "Turbulent Boundary Layer in Compressible Fluids," *Journal of the Aeronautical Sciences*, Vol. 18, 1951, pp. 145–160, 216.

[18] Clauser, F. H., "The Turbulent Boundary Layer," *Advances in Applied Mechanics*, Vol. 4, 1956, p. 1.

[19] Hornung, H. G., and Joubert, P. N., "The Mean Velocity Profile in Three-Dimensional Turbulent Boundary Layers," *Journal of Fluid Mechanics*, Vol. 15, 1963, pp. 368–385.

[20] Patel, V. C., "Calibration of the Preston Tube and Limitations on Its Use in Pressure Gradients," *Journal of Fluid Mechanics*, Vol. 23, 1965, pp. 185–208.

[21] Kim, K.-S., Lee, Y., and Settles, G. S., "Laser Interferometer/Preston Tube Skin-Friction Comparison in Shock/Boundary-Layer Interaction," *AIAA Journal*, Vol. 29, 1991, pp. 1007–1009.

[22] Anderson, S. D., and Eaton, J. K., "Reynolds Stress Development in Pressure-Driven Three-Dimensional Turbulent Boundary Layers," *Journal of Fluid Mechanics*, Vol. 202, 1989, pp. 263–294.

C. G. Speziale
Associate Editor